Spectroscopy of cross-conjugate nuclei ^{46}Ti–^{50}Cr and ^{47}V–^{49}Cr near the $f_{7/2}$-shell band termination

J. A. Cameron, J. L. Rodriguez, J. Jonkman,* G. Hackman,† S. M. Mullins,‡ C. E. Svensson, J. C. Waddington, and Lihong Yao
Department of Physics and Astronomy, McMaster University, Hamilton, Ontario, Canada L8S 4M1

T. E. Drake, M. Cromaz, J. H. DeGraaf, and G. Zwartz
Department of Physics, University of Toronto, Toronto, Ontario, Canada M5S 1A7

H. R. Andrews,§ G. Ball, A. Galindo-Uribarri,‖ V. P. Janzen, D. C. Radford,‖ and D. Ward¶
AECL Research, Chalk River Laboratories, Chalk River, Ontario, Canada K0J 1J0
(Received 24 September 1997)

High-spin states in the cross-conjugate pairs of nuclei ^{46}Ti–^{50}Cr and ^{47}V–^{49}Cr have been investigated using the reaction ^{28}Si+^{nat}Si at a laboratory energy of 125 MeV. Coincidence spectra, in some cases gated by charged particle detection, allow the yrast level schemes of all four nuclei to be extended, up to the $f_{7/2}$-shell band termination at 14^+ and $\frac{31}{2}^-$ in ^{46}Ti and ^{49}Cr, and beyond to 17^+ and $\frac{35}{2}^-$ in ^{50}Cr and ^{47}V. Opposite-parity bands in ^{46}Ti and ^{47}V were observed up to 11^- and $\frac{31}{2}^+$, respectively. Lifetimes derived from DSAM measurements provide $B(E2)$ and $B(M1)$ values for transitions among the higher levels of each of the nuclei. These are compared with earlier measurements and with $f_{7/2}$- and fp-shell model calculations. No model calculations have been published for the opposite-parity bands, but their level spacing and reduced transition rates support a spectator nature of the sd hole.
[S0556-2813(98)04008-4]

PACS number(s): 21.10.Tg, 23.20.Lv, 25.70.Gh, 27.40.+z

I. INTRODUCTION

Nuclei from ^{40}Ca to ^{56}Ni, in the shell model characterized by occupancy of the $f_{7/2}$ shell, display many properties which are well reproduced by such a simple model [1,2]. Spins and moments of most low-lying states are well represented, and the spectra of excitations display many of the features of the model, including, for example, band termination in nuclei near Ca and Ni, and cross-conjugate symmetry, a special feature of a major shell consisting of a single subshell. However, some features demand an enlarging of the shell model basis. The presence of bands of levels of opposite parity, particularly in the lighter nuclei near Ca, requires consideration of one-particle–one-hole $(1p-1h)$ excitations from the sd shell. At the other extreme, in the singly-closed-shell nuclei ^{52}Cr and ^{53}Mn, for instance, levels of the same parity but with spins exceeding the maximum allowed by $f_{7/2}$ nucleons alone have long been known, and excitations to the $p_{3/2}f_{5/2}p_{1/2}$ shell are required. Such excitations have also been invoked to account, through configuration mixing, for subtleties of the lower-level structures of other nuclei in the region [3]. Cross-conjugate symmetry, with its simultaneous neutron-proton and particle-hole exchange, leaves the Hamiltonian for a single $(nlj)^k$ model unchanged; so the level spectra of such pairs of nuclei are identical in this model and the corresponding components of their wave functions bear simple phase relations [2]. Accordingly, corresponding reduced $M1$ transition rates are identical. The relationship of $E2$ rates is more complicated, though strong resemblances remain, as the solid lines of Figs. 6(a) and 7, 8(a), and 9, below, show. In the nuclei considered here, the cross-conjugate pairs ^{46}Ti–^{50}Cr and ^{47}V–^{49}Cr, the level spectra and transition rates bear general resemblances, but differ in many details.

Finally, there is clear evidence for what is generally taken to be rotational behavior, both in the opposite-parity bands mentioned above and near midshell, in the nuclei ^{47}V, $^{47-49}$Cr, and ^{49}Mn. Here, the lowest several states follow a $J(J+1)$ energy dependence, and $B(E2)$ values are roughly twice those predicted by the $f_{7/2}$-shell model.

The results of earlier experimental studies of the midshell nuclei are accumulated in Refs. [4–8]. Most of the experiments were carried out almost 20 years ago, using relatively light projectiles on targets near ^{40}Ca and small detector arrays. These have the disadvantage of lower angular momentum, with resulting low intensity at the highest spins, and

*Present address: Department of Physics, University of Waterloo, Waterloo, Ontario, Canada N2L 3G1.
†Present address: Argonne National Laboratory, Argonne, IL 60439.
‡Present address: Department of Nuclear Physics, Research School of Physical Sciences and Engineering, Australian National University, Canberra, ACT, Australia.
§Present address: Bubble Technology Industries Inc., Chalk River, Ontario, Canada K0J 1J0.
‖Present address: Oak Ridge National Laboratory, Oak Ridge, TN 37831-6371.
¶Present address: Nuclear Science Division, Lawrence Berkeley Laboratory, Berkeley, CA 94720.

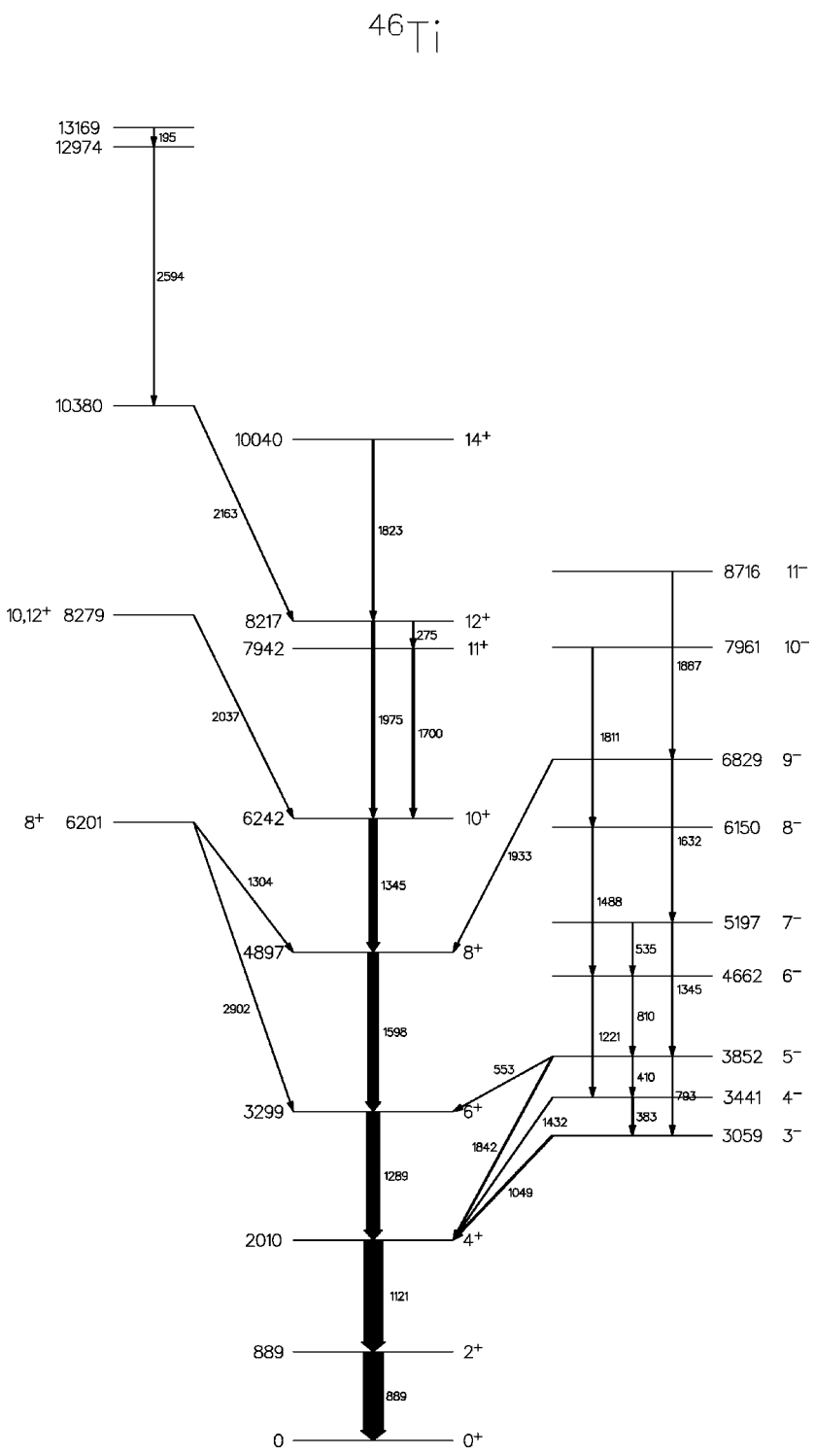

FIG. 1. Levels of ^{46}Ti from the present experiment.

small Doppler shifts for lifetime analysis. Their advantage for the latter use lies in the larger fraction of direct particle decay feeding to the levels. Experiments at McMaster [9], Daresbury [10–15], Chalk River [16,17], Legnaro [18,19], and Copenhagen [20], using large arrays of Compton-suppressed HPGe detectors, have investigated further the questions of band termination and midshell collectivity. In Ref. [9] the band-terminating level at $\frac{23}{2}^-$ in ^{51}Cr was identified and a few higher transitions were found. In the Daresbury experiments, the rotational structures first observed at low spin in ^{48,49}Cr [21] were seen to continue to higher spin in the five midshell nuclei ^{48}Cr and ^{48}Cr± 1 nucleon. A backbend was found in ^{48}Cr near $J=10$ and attributed to an $f_{7/2}$ rotation-induced alignment. At $J^\pi \simeq \frac{19}{2}^-$, the mirror pairs of odd-A neighbors of ^{48}Cr show a step in Coulomb energy differences, attributable to a similar alignment in the four-nucleon group. Pakou *et al.* [13] measured lifetimes in ^{49}Cr up to the 8-MeV level, and found that the g factor of the $\frac{19}{2}^-$ state is consistent with a collective interpretation. In ^{50}Cr, the g factors of the lowest four states remain near Z/A, as a

collective description would predict, whereas the $f_{7/2}$-shell model creates wide variations [15]. ^{50}Cr also presents an interesting anomaly in that the strong $E2$ transitions linking the yrast states are interrupted at the $12^+ \rightarrow 10^+$ transition. The sudden disappearance of $E2$ strength at this point indicates a shape change and requires the inclusion of upper pf configurations [22]. Recent advances in shell model technology have allowed calculations in the full fp model space [23–25]. In particular, these have shown that the ''collective'' properties of rotorlike energies, backbending, and large $B(E2)$ values can be reproduced. At the same time, these calculations appear to leave intact some of the properties associated with $f_{7/2}$-band termination, in particular, the reduction of $E2$ rates to a few Weisskopf units (W.u.).

High-spin studies of light nuclei are limited by the angular momentum that can be given to the compound nucleus in heavy-ion collisions. For example, ^{28}Si+^{28}Si at a center-of-mass energy of 60 MeV has a limiting angular momentum of about $40\hbar$ for peripheral collisions. At this energy ($E_x = 70$ MeV in ^{56}Ni) three or four nucleons or alpha particles are ejected, carrying up to $4\hbar$ per nucleon or $10\hbar$ per alpha and leaving the residue with under $20\hbar$ in most cases. It is therefore not surprising that most studies of f-shell nuclei have been limited to spins not much higher than $10\hbar$.

Two further factors make it difficult to pursue the spectroscopy to higher spins. The low mass of the nuclei implies high recoil velocities from heavy-ion reactions ($v/c \sim 5\%$). Together with the high energy of gamma rays (~ 2 MeV at $J \simeq 12$) this gives rise to large Doppler broadening. The low Coulomb barrier in light systems implies that charged particle exit channels are little hindered; so in a typical reaction ten or more channels are found in significant strength. There is therefore considerable channel cross talk in the spectroscopy.

In spite of these difficulties, it has been possible, using the ^{28}Si+^{28}Si reaction, with both self-supporting and backed targets, to advance considerably the spectroscopy of many nuclei from ^{44}Ti to ^{53}Mn. New transitions and levels have been found, and for many levels spin assignments and lifetimes have been determined. A first result from this experiment, the levels and lifetimes in ^{48}Cr up to $J^\pi = 16^+$, has been published [17]. Here we present results for two cross-conjugate pairs of nuclei, ^{46}Ti–^{50}Cr and ^{47}V–^{49}Cr.

II. EXPERIMENT

The experiments were made at Atomic Energy of Canada's former Chalk River Laboratory TASCC, using the 8π gamma spectrometer. A self-supporting natural Si target (92% ^{28}Si, 5% ^{29}Si, 3% ^{30}Si), consisting of two separated 500 μg/cm^2 layers, was used to establish the level schemes. In addition to coincidences in the 20-element Ge array, at least two further gamma-ray events were required of the BGO array and charged particles were detected in the 44-element CsI detector. The nuclei ^{46}Ti, ^{50}Cr, ^{47}V, and ^{49}Cr are produced in the $2\alpha 2p$, $\alpha 2p$, $2\alpha p$, and $\alpha 2pn$ exit channels following ^{28}Si+ ^{28}Si fusion at a laboratory energy of 125 MeV. Although in the present case the reaction channels were strong and channel selection was not needed to enhance their presence against background, the improvement in resolution coming from kinematic reconstruction of each detected event was helpful [17]. For lifetime measurements, a target of 800 μg/cm^2 of Si deposited on a gold backing was used, without charged particle detection. Full gamma-gamma matrices were constructed for coincidence spectroscopy, and angle-selected matrices for angular correlation and lifetime analysis.

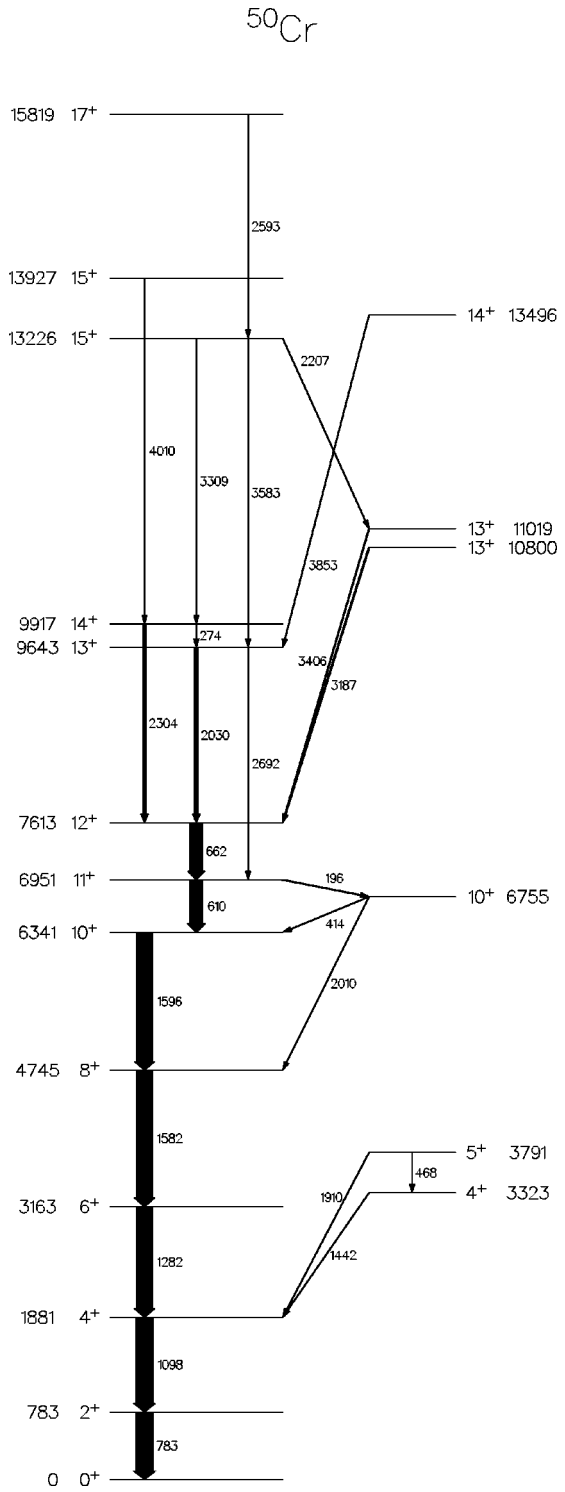

FIG. 2. Levels of ^{50}Cr from the present experiment.

Energy calibration was made using sources of ^{152}Eu, ^{60}Co, and ^{88}Y. In the range covered by these, energy measurements are precise to about 1 keV, but are somewhat poorer beyond 2 MeV, partly as a result of the necessary

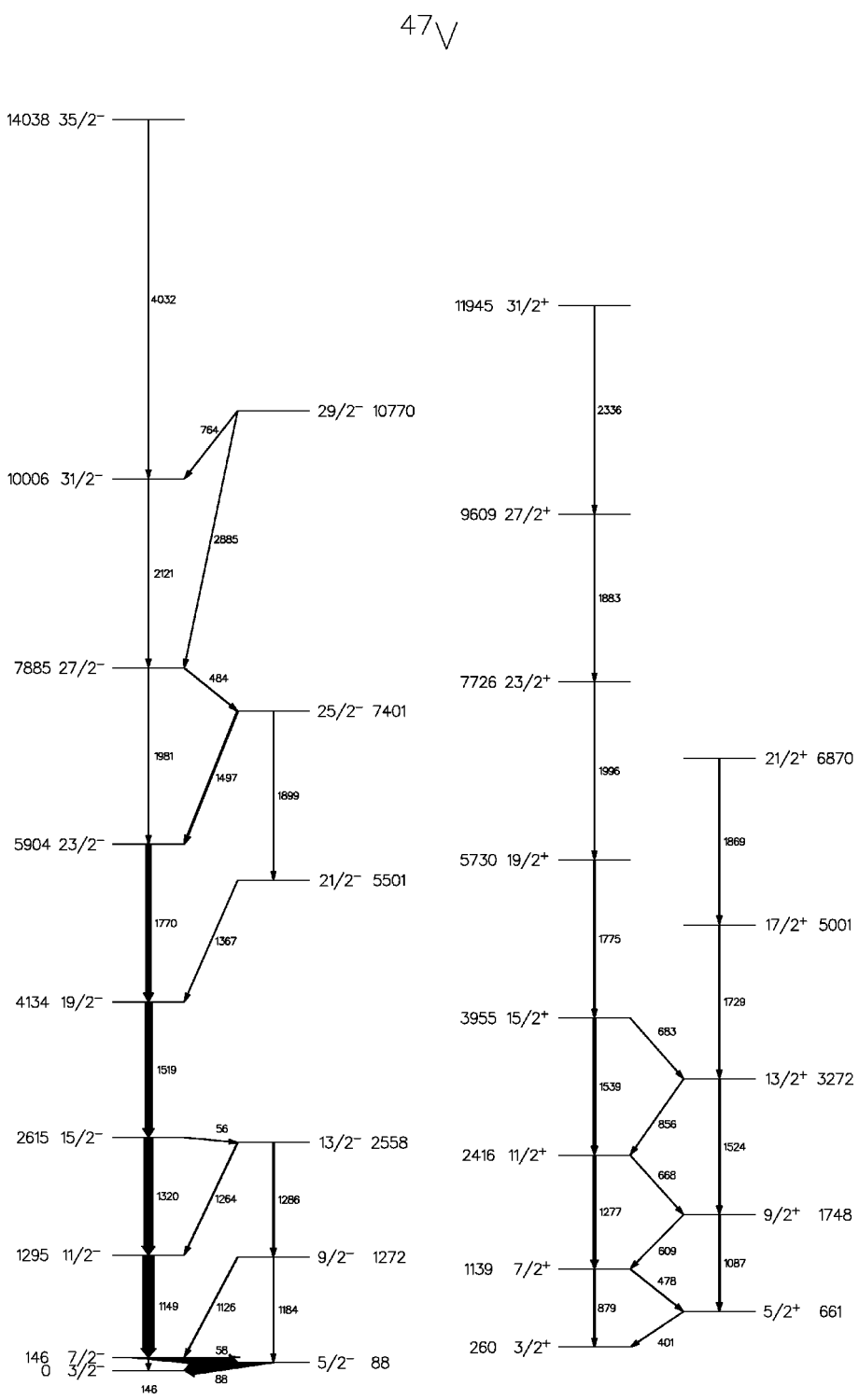

FIG. 3. Levels of ^{47}V from the present experiment. The transitions connecting the two bands are not shown. They are given in Ref. [5] and included in Table II.

extrapolation of the calibration, but to a large extent due to the kinematic broadening of the reaction lines. With the self-supporting target, after reconstruction using the charged particle detection, the line width at high energy was about 0.7% full width at half maximum (FWHM). From the backed target data, lines showing an appreciable stopped component were also used in the energy determinations.

Spin determinations rely on γ-ray angular distributions. The four 5-detector rings of the 8π spectrometer are at polar angles of 37° and 79°, and the supplementary angles 101° and 143°; so only a single number is available from angular distribution (AD) measurements. Whether in singles or coincidence with a γ_1 detected at all angles, the angular anisotropy

$$A = W[\gamma_2(37)]/W[\gamma_2(79)]$$

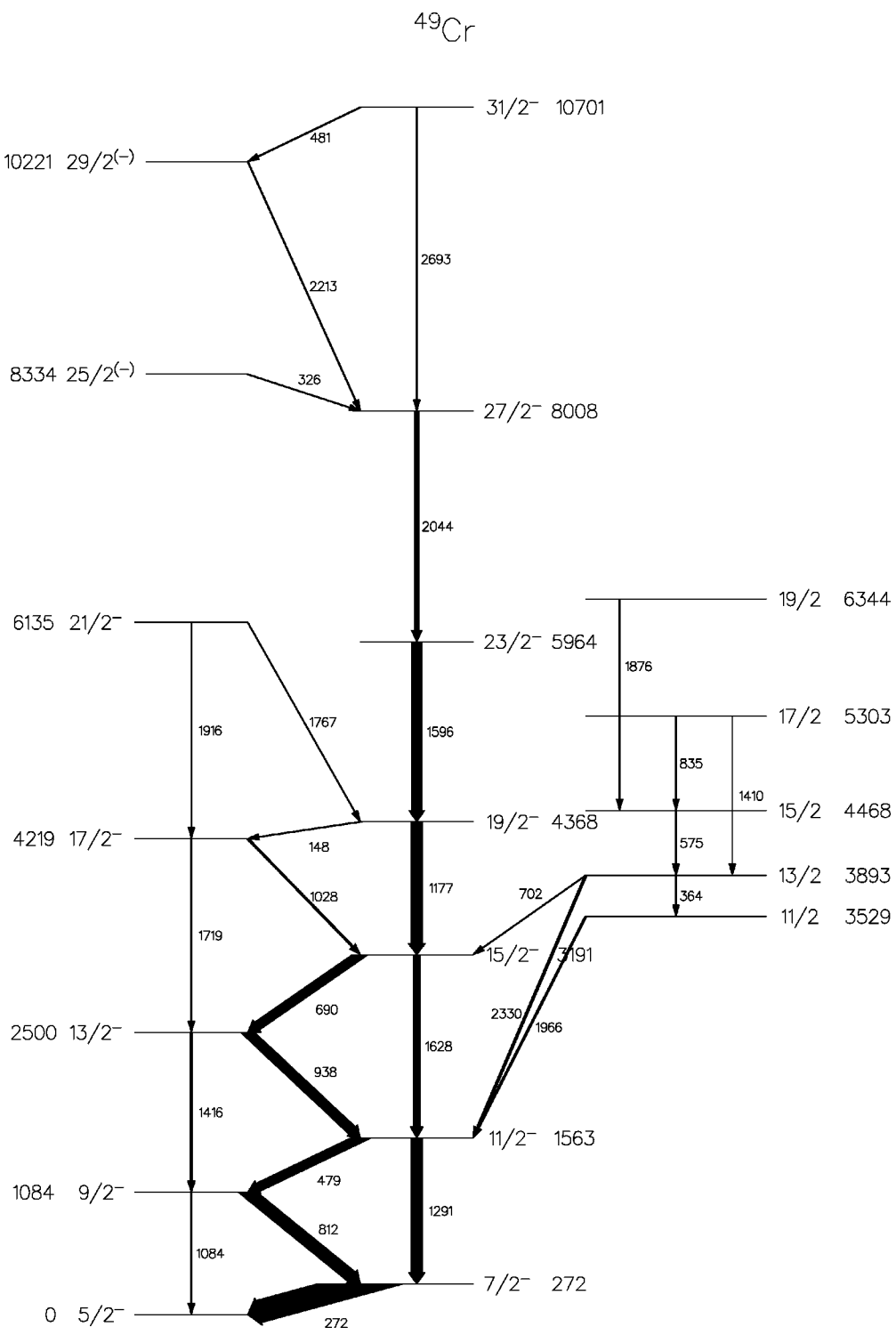

FIG. 4. Levels of ^{49}Cr from the present experiment.

is ~ 0.8 for $J+1 \overset{D}{\rightarrow} J$ and ~ 1.5 for $J+2 \overset{Q}{\rightarrow} J$ and for $J \overset{D}{\rightarrow} J$. The arrows $\overset{D}{\rightarrow}$ and $\overset{Q}{\rightarrow}$ represent pure dipole and quadrupole transitions. Directional correlations of oriented nuclei (DCO), with both γ_1 and γ_2 in single rings of the array, allow inference of spin sequences in gamma-gamma coincidences. The DCO ratio, defined as

$$R = W[\gamma_1(37)\,\gamma_2(79)]/W[\gamma_1(79)\,\gamma_2(37)],$$

has values for stretched dipole and quadrupole γ_2 transitions of ~ 1 and ~ 1.5 for a dipole γ_1 and ~ 0.5 and ~ 1 for a quadrupole γ_1. It suffers the same discrete ambiguity, between $J+2 \overset{Q}{\rightarrow} J$ and $J \overset{D}{\rightarrow} J$, found in the angular anisotropy of intensity. Selection between the two inferences depends on the observation (or lack thereof) of the crossover transition or on a measurement of the transition rate.

The decay rates of levels strongly populated in the Si+Si reaction were found from analysis of the Doppler-shifted

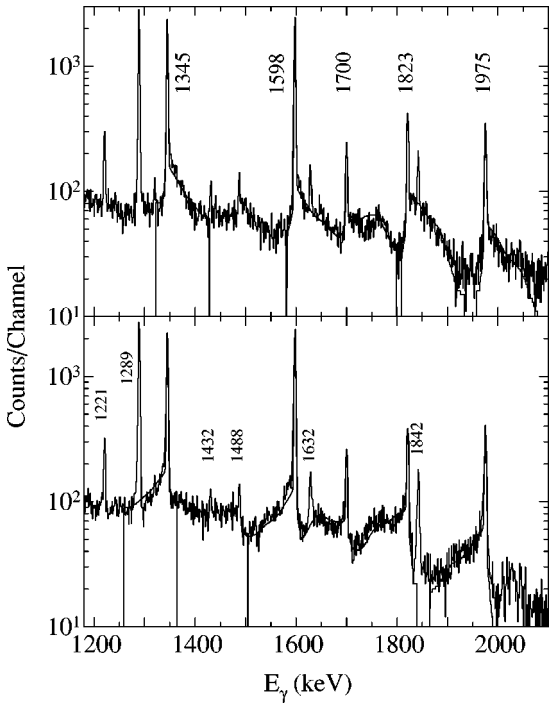

FIG. 5. Part of the backed target spectra at 37° (top) and 143° (bottom) for ^{46}Ti, summed from spectra gated by the 889-, 1121-, and 1298-keV γ rays, with the computed fits for the yrast lines. These are labeled in the upper part. The labels in the lower part are for the decays of the yrast 6^+ and some of the negative-parity states.

gamma rays from the nuclei recoiling in the gold-backed target. In order to extract $F(\tau)$ values, gamma energy centroids were measured at all four angles and fitted to the form

$$E_\gamma(\theta) = E_\gamma(90)\left(1 + F(\tau)\frac{v}{c}\cos(\theta)\right).$$

Here, v is the initial recoil velocity and $F(\tau)$ is the ratio of the velocity-averaged Doppler shift to the full shift. In most cases it was also possible to fit the 37° and 143° line shapes using a DSAM code designed for multilevel, nonrotational, level systems [26]. Uncertainties which enter such comparisons have several sources. The recoil dynamics must be modeled, using stopping-power data. In the present analysis the electronic stopping-power tables of Northcliffe and Schilling [27] were used, together with Blaugrund's analytical correction for nuclear stopping [28]. A comparison was made with stopping powers calculated from the Monte Carlo code TRIM [29], but little difference was found. In analyzing DSAM spectra for such light recoil ions, account must be taken of the large kinematic broadening effects. These arise from the reaction kinematics itself, whereby the recoil ions occupy a cone of significant opening angle and from the large-angle scattering of the ions as they slow down in a backing of much heavier atoms. Such effects are exacerbated in modern arrays where the detectors are not on the beam axis. In the present analysis, both these effects were simulated using a semiempirical velocity-dependent line-broadening function. Where this function is symmetric, it does not affect the computed value of the attenuation factor $F(\tau)$, but it does affect higher moments of the computed line shape.

The most important uncertainties in some decay rates arise from the level scheme itself. Because the levels form part of a cascade, the time evolution of the population of any level depends on the lifetimes of the level in question and of all those through which it is fed, including unobserved ones. It is customary, in addressing this problem in heavier rotational nuclei, to assume that top- and side-feeding levels are continuous extensions of the known bands, and that their decay rates may be extrapolated from the measured ones. In the present analysis, this assumption is questionable, given

TABLE I. Transitions in ^{46}Ti.

Level (MeV)	$F(\tau)$	τ (ps)	J_i^π	J_f^π	E_γ (MeV)	I_γ	AD	DCO	BR (%)	$T(E2)$ (W.u.)	$T(M1)$ (W.u.)	$T(E1)$ (mW.u.)
4.897	0.10(3)*	1.33(33)	8^+	6^+	1.598	100	1.53(3)	0.94(3)	100	6.3(16)		
6.201	0.68(4)	<0.28	8^+	6^+	2.902	5.7			60	>0.86		
				8^+	1.304	3.7			40		>0.02	
6.242	0.07(1)*	2.5(6)	10^+	8^+	1.345	75	1.50(2)	0.95(5)	100	7.5(19)		
7.942	0.46(3)*	<0.1	11^+	10^+	1.700	17	0.69(2)	0.65(4)	100		>0.13	
8.217	0.20(2)*	0.83(8)	12^+	10^+	1.975	21	1.33(4)	0.8(1)	70	2.3(2)		
				11^+	0.275	9.4			30		0.56(6)	
8.279	0.74(7)	<0.24	$10,12^+$	10^+	2.037	1.8	0.97(5)		100	>9.5	>0.015	
10.040	0.38(6)*	<0.9	14^+	12^+	1.823	11	1.44(3)	1.0(1)	100	>4.4		
6.150	0.15(2)*	0.43(4)	8^-	6^-	1.734	1.8			14	1.7(2) [a]		
				6^-	1.488	11	1.35(6)	1.5(2) D	86	22(2)		
6.829	0.27(4)*	0.76(15)	9^-	8^+	1.933	1.8			14			0.019(4)
				7^-	1.632	11	1.4(2)		86	8(2)		
7.961	0.55(1)*	<0.44	10^-	8^-	1.811	11	1.43(6)	1.2(2) D	100	>9.7		
8.716	0.48(5)	<0.42	11^-	9^-	1.887	5.5		0.9(2)	100	>5.8		

[a]Final state 4.416 MeV [3,10].

TABLE II. Transitions in ^{50}Cr.

Level (MeV)	$F(\tau)$	τ (ps)	J_f^π		E_γ (MeV)	I_γ	AD	DCO	BR (%)	$T(E2)$ (W.u.)	$T(M1)$ (W.u.)
6.755	0.26(5)	$0.16(^{+13}_{-10})$	10^+	8^+	2.010	3.8	1.08(18)		40	$6(^{+9}_{-3})$	
				10^+	0.414	5.8			60		2^{+2}_{-1}
6.951	0.18(2)*	0.83(14)	11^+	10^+	0.610	100	0.73(1)	0.56(2)	92		0.16(2)
				10^+	0.196	8.8			8		0.40(7)
7.613	0.50(1)*	0.24(3)	12^+	10^+	1.272	<2			<2	<2	
				10^+	0.858	<2			<2	<15	
				11^+	0.662	95	0.79(1)	0.53(2)	100		0.46(6)
9.643	0.90(3)*	0.07(3)	13^+	11^+	2.692	4.0	1.79(6)		12	$0.9(^{+6}_{-3})$	
				12^+	2.030	31	1.22(3)	0.44(6)	88		$0.051(^{+30}_{-15})$
9.917	0.58(2)*	0.37(4)	14^+	12^+	2.304	23	1.75(5)	1.25(10)	76	2.3(3)	
				13^+	0.274	7.3	0.7(2)		24		1.0(2)
10.800	0.38(2)	<0.9	13^+	12^+	3.187	11	1.11(5)	0.55(5)	100		>0.001
11.019	0.84(1)	0.086(14)	13^+	12^+	3.406	7.4	0.76(4)		100		0.009(2)
13.226	0.93(1)	$0.031(^{+10}_{-6})$	15^+	13^+	3.583	4.1	1.74(12)		33	1.3(3)	
				14^+	3.309	3.1			25		0.007(2)
				13^+	2.207	5.2		1.2(2)	42	19(5)	
13.496			14^+	13^+	3.853	1.1			100		
13.927	0.90(1)	<0.11	15^+	14^+	4.010	3.2	0.97(7)	1.2(4)	100		>0.005
15.819	0.94(2)*	<0.07	17^+	15^+	2.593	9.2	1.4(2)	1.0(1)	100	>9	

the underlying independent-particle structure. As a reasonable alternative, these unobserved transitions were assumed to be rapid ($\tau<10$ fs). The rationale is that the failure to observe the feeding transitions implies that they are direct particle or high-energy (>4 MeV) gamma decays. In addition, decay rate uncertainties contain a contribution from those of the measured intensities, since these affect the detailed level histories. In most cases, therefore, precision better than 10% is unlikely near the top of the level scheme. The highest observed level of a sequence presents a particular case, in that its measured mean time to decay includes those of the preceding unobserved states. Accordingly, the decay rates attributed to such levels are shown only as lower limits.

Because of the accumulation of uncertainties in the descent through the level scheme, lower-level decay rates are mostly of lower precision, in spite of their greater intensity. An ironical consequence of this is that, in some cases, heavy-ion measurements of lifetimes may not extend as low in the level scheme as the upper limits from earlier measurements with light projectiles.

III. RESULTS

Approximately 15×10^6 events were accumulated in each of the experiments, sufficient to allow new levels to be found, spins to be determined, and in many cases lifetimes to be measured. Level schemes found for the four nuclides ^{46}Ti, ^{50}Cr, ^{47}V, and ^{49}Cr are shown in Figs. 1–4, respectively. Figure 5 is an example of the backed target coincidence spectra obtained, in this instance for ^{46}Ti. It contains spectra summed over the 37° and 143° detector rings in coincidence with any of the lowest three transitions in the positive-parity band. The energies of γ transitions above these are marked on the upper spectra, while one of the gating transitions (1289 keV) and five lines originating in the negative-parity band are marked below. Computed line shapes for the positive-parity band are shown for both spectra. Tables I–IV contain the details of relative γ-ray intensities, angular anisotropies, and DCO ratios, and derived branching ratios (BR's) and lifetime values, with their inferred partial decay rates. Unobserved but possible dipole and quadrupole transitions are included with estimates of their upper limits of intensity. The asterisks in the $F(\tau)$ columns indicate that a full line shape analysis was made. The DCO ratios were most commonly based on gates known to be $J+2\overset{Q}{\rightarrow}J$ in character. The few exceptions of gates $J+1\overset{D}{\rightarrow}J$ are marked ''D.'' The ratios of transition rates to Weisskopf single-particle estimates allow comparison with general trends [30]. In Figs. 6–9 experiment and shell model theory [2,22–25] are directly compared for the yrast transitions.

A. ^{46}Ti

The level scheme proposed in Refs. [4] and [11] was reexamined. What had previously been taken to be a second 12^+ level, at 10040 keV, on the basis of the angular distribution of its 1823-keV decay to the 12^+ 8217-keV level and of a 2100-keV transition, apparently to the 7942-keV 11^+ level, is more likely to be the band-terminating 14^+ state. The angular anisotropy and DCO measurements do not disagree with the 12^+ interpretation, but also allow a 14^+ assignment. The placement of the 2100-keV gamma ray is therefore crucial. In the coincidence spectra taken with the backed target, the 1823-keV peak [$F(\tau)=0.38(6)$] has a distinct stopped component, whereas the 2100-keV line [$F(\tau)>0.96$] does not; so the latter cannot be a second branch from the 10042-keV level.

TABLE III. Transitions in ^{47}V.

Level (MeV)	$F(\tau)$	τ (ps)	J_i^π	J_f^π	E_γ (MeV)	I_γ	AD	DCO	BR (%)	$T(E2)$ (W.u.)	$T(M1)$ (W.u.)	$T(E1)$ (mW.u.)
2.615	<0.03	>2.5	$\frac{15}{2}^-$	$\frac{11}{2}^-$	1.320	100	1.39(1)	1.13(5)	98	<9		
				$\frac{13}{2}^-$	0.056	1.9			2		<3	
4.134	0.16(1)*	0.70(10)	$\frac{19}{2}^-$	$\frac{15}{2}^-$	1.519	80			100	14(2)		
5.501	0.39(4)	0.07(4)	$\frac{21}{2}^-$	$\frac{19}{2}^-$	1.367	2.0			100		0.27(16)	
5.904	0.30(1)*	0.50(7)	$\frac{23}{2}^-$	$\frac{19}{2}^-$	1.770	59	1.49(1)	1.16(4)	100	10(2)		
				$\frac{21}{2}^-$	0.403	<3			<5		<0.06	
7.401	0.46(3)	0.34(5)	$\frac{25}{2}^-$	$\frac{21}{2}^-$	1.900	2.1			10	1.0(2)		
				$\frac{23}{2}^-$	1.497	18	0.90(4)		90		0.025(4)	
7.885	0.53(1)*	0.14(3)	$\frac{27}{2}^-$	$\frac{23}{2}^-$	1.981	10		1.0(1)	55	12(3)		
				$\frac{25}{2}^-$	0.484	8.2	0.81(1)	0.58(5)	45		1.0(3)	
10.006	0.51(1)*	0.34(4)	$\frac{31}{2}^-$	$\frac{27}{2}^-$	2.121	10	1.40(2)	1.2(1)	100	5.4(6)		
10.770	0.82(1)	<0.14	$\frac{29}{2}^-$	$\frac{27}{2}^-$	2.885	4.1	1.08(4)		67		>0.0065	
				$\frac{31}{2}^-$	0.764	2.0	1.09(4)		33		>0.17	
14.038	0.85(2)	<0.12	$\frac{35}{2}^-$	$\frac{31}{2}^-$	4.032	3.9	1.57(13)		100	>0.6		
2.416	0.07(1)*	1.4(6)	$\frac{11}{2}^+$	$\frac{7}{2}^+$	1.277	17	1.76(3)		86	14(6)		
				$\frac{9}{2}^+$	0.668	2.0	0.58(6)		11		0.008(4)	
				$\frac{9}{2}^-$	1.144	0.5			3			0.011(6)
3.272	<0.1	>3	$\frac{13}{2}^+$	$\frac{9}{2}^+$	1.524	8.1			80	<2.5		
				$\frac{11}{2}^+$	0.856	1.5			15		<0.003	
				$\frac{11}{2}^-$	1.977	0.5			5			<0.002
3.955	0.25(3)*	0.54(9)	$\frac{15}{2}^+$	$\frac{11}{2}^+$	1.539	11	1.8(1)		92	24(5)		
				$\frac{13}{2}^+$	0.683	1.0			8		0.024(6)	
5.001			$\frac{17}{2}^+$	$\frac{13}{2}^+$	1.729	4.5			100			
5.730	0.44(3)*	0.33(6)	$\frac{19}{2}^+$	$\frac{15}{2}^+$	1.775	5.9	1.50(5)		100	$13(^{+2}_{-4})$		
				$\frac{17}{2}^+$	0.729	<0.6			<10		<0.025	
6.870			$\frac{21}{2}^+$	$\frac{17}{2}^+$	1.869	1.2	1.54(6)		100			
7.726	0.68(3)	<0.1	$\frac{23}{2}^+$	$\frac{19}{2}^+$	1.996	1.8			100	>25		
9.609	0.69(9)*	0.12(5)	$\frac{27}{2}^+$	$\frac{23}{2}^+$	1.883	2.2		1.9(2) D	100	30(12)		
11.945	0.76(4)*	<0.17	$\frac{31}{2}^+$	$\frac{27}{2}^+$	2.336	1.7	1.56(4)	2.6(5) D	100	>8		

Neither angular distribution nor lifetime measurements were possible for the weak side-feeding transitions earlier identified [11] nor for three new ones found feeding the 12^+ state. If these have increasing spin, then further levels with spins greater than 13 are implied at 12984 and 13179 keV, respectively. These are accommodated up to spin 16 by single excitations to the upper pf shell. The negative-parity band, which would not be expected to terminate until about 18^-, was seen only to 11^-, this latter spin being confirmed by the DCO measurements.

Most of the ^{46}Ti levels and lifetimes observed in the present experiment have been found previously [4,31]. For the most part, the agreement is satisfactory, the two marked exceptions being for the 8^+ and 10^+ levels. The 10^+ level obtains almost half its population through side feeding, which is assumed to be rapid in the present analysis, for the reasons given above. The discrepancy can be removed for this level, with only a small reduction in the goodness of fit, by assuming a mean lifetime of the side feed to this level of about 1.5 ps, consistent with the assumption made by Rammo *et al.* [4,31]. The result for the 8^+ level is not changed significantly by this, and remains lower than that obtained previously by the same group. The principal changes are the reassignment of the spin of the 10040-keV level and the consequent interpretation of its decay rate. The assignment of $J^\pi = 11^-$ to the 8716-keV level confirms this inference in Ref. [11]. The decay rates of this state and of the 10^- state are new.

B. ^{50}Cr

Previous heavy-ion experiments [8] established the yrast sequence up to the 12^+ 7613-keV state. The band-terminating states 13^+ and 14^+ were found by Rodriguez at 9643 and 9917 keV [16]. Higher transitions were also seen in his ^{40}Ca(^{12}C,$2p$) and ^{40}Ca(^{16}O,$\alpha 2p$) reactions. The higher angular momentum available in the Si+Si reaction increased the intensity of feeding through these levels so that AD and DCO measurements could be made. Consequently, spins up to 16^+ were established. A search for the weak 1272-keV

TABLE IV. Transitions in ^{49}Cr.

Level (MeV)	$F(\tau)$	τ (ps)	J_i^π	J_f^π	E_γ (MeV)	I_γ	AD	DCO	BR (%)	$T(E2)$ (W.u.)	$T(M1)$ (W.u.)	$T(E1)$ (mW.u.)
4.219	0.42(5)*	0.22(3)	$\frac{17}{2}^-$	$\frac{13}{2}^-$	1.719	4.1	1.13(10)		27	6.6(10)		
				$\frac{15}{2}^-$	1.028	11	0.87(3)	0.8(2) D	73		0.10(2)	
4.368	0.04(1)*	2.5(6)	$\frac{19}{2}^-$	$\frac{15}{2}^-$	1.177	100	1.38(1)	1.04(7)	96	14(3)		
				$\frac{17}{2}^-$	0.148	4.2	0.91(1)	0.55(6)	4		0.16(4)	
5.964	0.24(1)*	0.65(7)	$\frac{23}{2}^-$	$\frac{19}{2}^-$	1.596	90	1.49(2)	1.3(1)	100	13(2)		
6.135	<0.04	>9	$\frac{21}{2}^-$	$\frac{17}{2}^-$	1.916	2.7			67	<0.2		
				$\frac{19}{2}^-$	1.767	1.4			33		<0.0002	
				$\frac{23}{2}^-$	0.171	<0.4			<10		<0.07	
8.008	0.57(1)*	0.27(3)	$\frac{27}{2}^-$	$\frac{23}{2}^-$	2.044	56	1.50(2)	1.2(1)	100	8.5(9)		
8.334	0.53(1)	<0.43	$\frac{25}{2}^{(-)}$	$\frac{23}{2}^-$	2.370	<10			<20			
				$\frac{21}{2}^-$	2.199	<8			<15			
				$\frac{27}{2}^-$	0.326	3.2	0.97(4)	0.6(1)	100		>1.6	>40
10.221	0.94(2)*	0.045(15)	$\frac{29}{2}^{(-)}$	$\frac{27}{2}^-$	2.213	13	0.70(2)		100		0.07(3)	19(6)
				$\frac{25}{2}^{(-)}$	1.890	<1			<10	<8		
10.701	0.91(4)*	<0.12	$\frac{31}{2}^-$	$\frac{27}{2}^-$	2.693	9.2	1.38(5)		88	>4		
				$\frac{29}{2}^{(-)}$	0.477	1.3	0.96(6)		12		>0.3	>6
3.529	<0.06	>4	$\frac{11}{2}$	$\frac{11}{2}^-$	1.966	7.9	0.88(4)		100		<0.001	<0.025
3.893	<0.04	>4	$\frac{13}{2}$	$\frac{11}{2}^-$	2.330	13	0.82(3)		80		<0.0005	<0.012
				$\frac{15}{2}^-$	0.702	1.3	0.89(6)		8		<0.002	<0.05
				$\frac{11}{2}$	0.364	1.9			12		<0.02	<0.5
4.468	<0.04	>4	$\frac{15}{2}$	$\frac{13}{2}$	0.575	8.9	0.60(2)		100		<0.05	<1
5.303	<0.02	>4	$\frac{17}{2}$	$\frac{13}{2}$	1.410	1.2	1.3(3)		45	<1.5		
				$\frac{15}{2}$	0.835	1.5	0.54(3)		55		<0.008	<0.2
6.344	0.52(2)	<0.44	$\frac{19}{2}$	$\frac{15}{2}$	1.876	7.8			100	>7		

$12^+ \rightarrow 10^+$ transition leads to an upper limit on its intensity amounting to 2% of the 662-keV dipole cascade decay.

The highest state observed, at 15819 keV, has been assigned spin 17^+ since it reaches the 15^+ level by a stretched quadrupole transition. All of the transitions above the 12^+ 9917-keV state are quite rapid. This is not surprising, since their energies are high. The 3187-keV dipole transition from the 10.8-MeV level presents an interesting exception, in that it appears to be quite slow. The lifetime limit assigned to this state in Table II may be that of an unobserved parent.

A recent spectroscopic study at Legnaro using the ^{24}Mg $+^{28}$Si reaction with a self-supporting target reports all of these levels and several more [19]. Most of the present spin determinations are in agreement with that work. Exceptions are the 13496-keV level, not reported from Legnaro, and the spin of the 15819-keV level, reported there as 16^+. Also in the Legnaro findings are a low-energy quadrupole preceding the 3187-keV dipole mentioned above and a 3% crossover transition from 12^+ to 10^+.

C. ^{47}V

Several new transitions feeding high-lying levels in ^{47}V were found. One of these, at $E_\gamma = 4032$ keV, feeds the $f_{7/2}$ band-terminating $\frac{31}{2}^-$ state. Its angular anisotropy suggests that it is a stretched quadrupole transition. No 3270-keV transition leading to the $\frac{29}{2}^-$ state, expected for the alternative interpretation as a second $\frac{31}{2}$, was found. The $\frac{21}{2}^-$ level, previously missing, has been located at 5501 keV. Because the transition connecting it to the $\frac{23}{2}^-$ state has not been found, and the intensities of the 1367- and 1899-keV lines are about equal, their assigned order depends on their relative $F(\tau)$ values. Previous measurements of lifetimes extend only to the $\frac{11}{2}^-$ state, whereas the present DSAM results extend from $\frac{15}{2}^-$ to $\frac{35}{2}^-$. No lifetime measurement exists for the $\frac{13}{2}^-$ state at 2558 keV.

The present measurements extend the positive-parity band to $\frac{31}{2}^+$, with lifetimes from $\frac{11}{2}^+$ to $\frac{31}{2}^+$.

D. ^{49}Cr

The present measurements extend and revise the yrast band, and lifetimes have been obtained up to the 10.7-MeV $f_{7/2}$-band-terminating state. Pakou *et al.* [13] reported similar measurements for yrast states up to 8 MeV. The present results are generally in agreement with these, with the exception of the lifetime of the 5.9-MeV level. The level at 5964 keV was previously assigned as a second $\frac{19}{2}^-$ state, based on the angular distribution of its 1596-keV decay to the yrast $\frac{19}{2}^-$ state, together with the observation of a weak 1745-keV transition, presumed to be leading to the $\frac{17}{2}^-$ level [11]. This gamma ray was not seen in the present coincidence spectra,

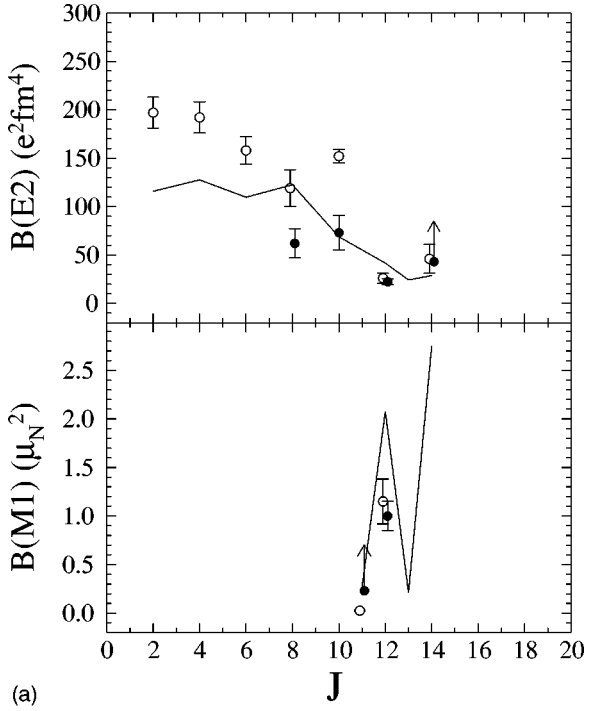

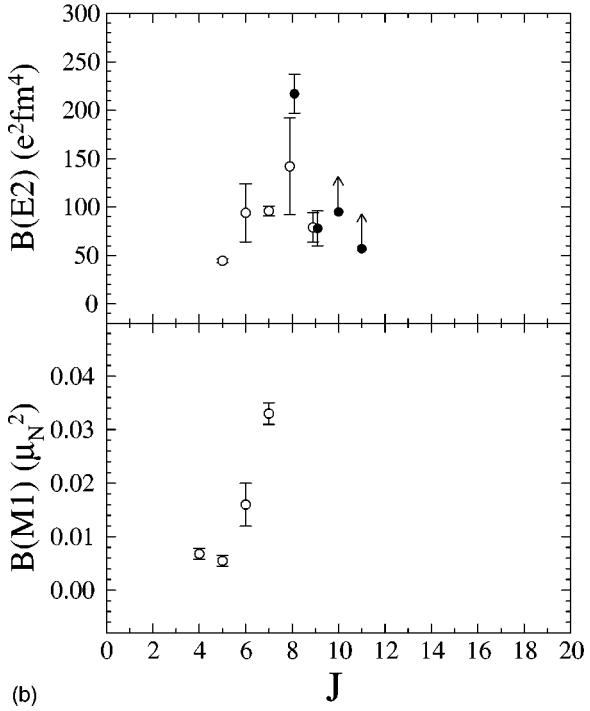

FIG. 6. Reduced rates $B(E2)_{J\to J-2}(e^2\ \mathrm{fm}^4)$ and $B(M1)_{J\to J-1}(\mu_n^2)$ for yrast transitions in ^{46}Ti: (a) positive-parity band, (b) negative-parity band. Solid circles: present results. Open circles: Ref. [4]. Solid line: $f_{7/2}^k$-shell model [2].

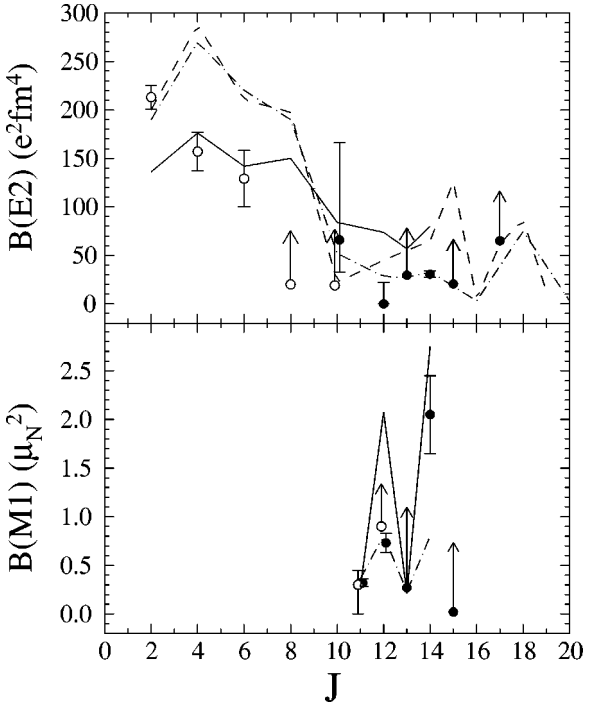

FIG. 7. Reduced rates for yrast transitions in ^{50}Cr. Open circles: Ref. [8]. Dashed line: fp shell model [22]. Dash-dotted line: fp-shell model [24] [odd-$JB(E2)$'s are not given for $J>11$]. See the text for the distinction between these. Other details as in Fig. 5.

nor was a transition between the 8008- and 4368-keV levels. It therefore seems more probable that the 5964-keV level is in fact the yrast $\frac{23}{2}^-$ state, and that the 8008-, 10221-, and 10701-keV levels should be reassigned as $\frac{27}{2}^-$, $\frac{29}{2}^-$, and $\frac{31}{2}^-$, respectively. A new 326-keV stretched dipole transition was found feeding the 8008-keV level. Its parent, at 8334 keV, is tentatively assigned as the yrast $\frac{25}{2}^-$ state. The expected quadrupole transitions connecting it to the $\frac{29}{2}^-$ and $\frac{21}{2}^-$ levels were not observed; so the parity is uncertain. However, the decay rate favors negative parity since alternatively an $E1$ rate would exceed other values found in the region [30]. It is interesting that the $f_{7/2}$ and fp models predict these $E2$ transitions to be slow and the $M1$ decay to be fast (Fig. 8).

In Ref. [11], a weakly populated side structure was reported. The coincidences found here support this but place several of the gamma transitions differently. The parity of this group of levels, which form a rotorlike band from $\frac{11}{2}$ to $\frac{19}{2}$, is also uncertain. Within the group, the quadrupole transitions indicate the same parity for the $\frac{13}{2}$-$\frac{17}{2}$ and $\frac{15}{2}$-$\frac{19}{2}$ pairs, but the dipole transition rates are not decisive between $M1$ and $E1$. The interband dipole transitions, whether regarded as $M1$ or $E1$ in character, are greatly retarded, as in the case of ^{48}Cr [6,17]. Such retardation is not unprecedented in this region [30]. The energy scale of the band is represented by a moment of inertia parameter $\hbar^2/2\mathfrak{I}=27$ keV, half that associated with the lower levels of the yrast band. On the other hand, the reduced $E2$ rates are comparable to those in the yrast band. Levels closely corresponding to these are to be found among the yrare levels of the $f_{7/2}$- and fp-shell models [2,25].

IV. DISCUSSION

The level schemes and decay rates in each of the nuclei studied here have many similar features. Although there is considerable variation in detail, it is apparent that for all, including the sd-hole bands in ^{46}Ti and ^{47}V, there is a smooth decrease of the moment of inertia parameter $\hbar^2/2\mathcal{J}^{(1)}$ from 70 keV at $J\simeq 4$ to 40 keV at $J\simeq 12$, rising again to 50 keV at $J\simeq 16$, the $f_{7/2}$-band termination. (The rigid sphere

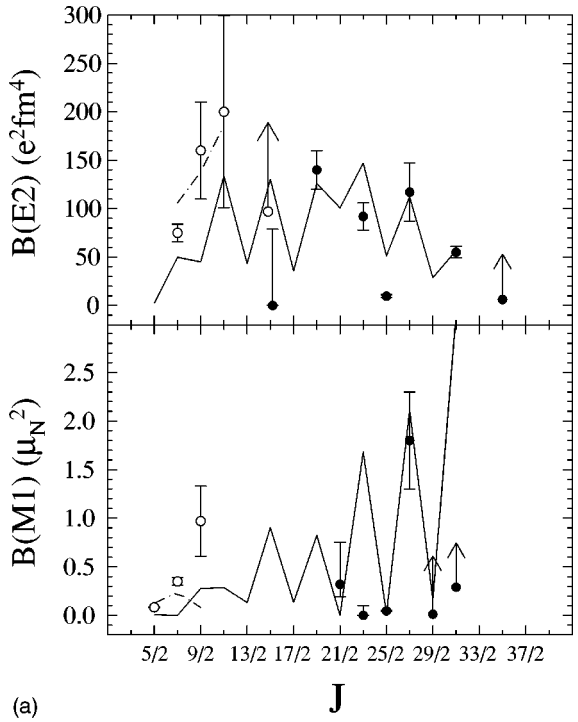

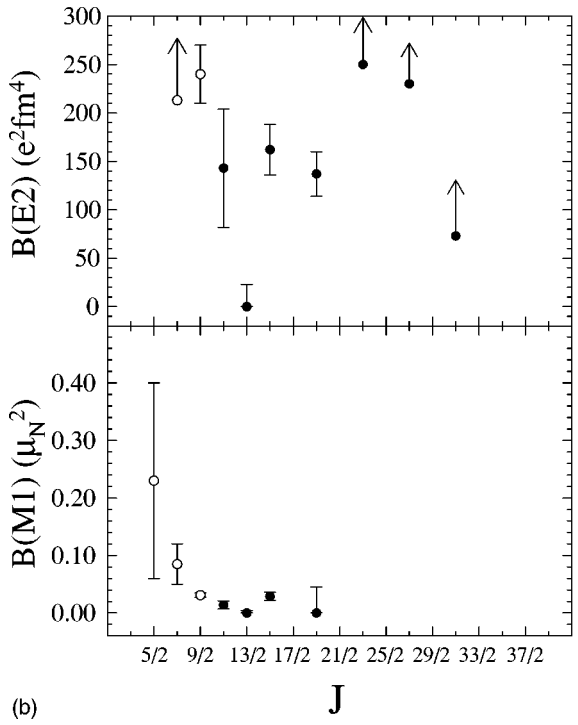

FIG. 8. Reduced rates for yrast transitions in ^{47}V. (a) Negative-parity band, (b) positive-parity band. Open circles: Ref. [5]. Dash-dotted line: fp-shell model [25]. Other details as in Figs. 5 and 6.

value of $\hbar^2/2\mathcal{J}^{(1)}$ is 42 keV at $A=48$.)

A comparison of the reduced transition rates for the pairs ^{46}Ti–^{50}Cr [Figs. 5(a) and 6] and ^{47}V–^{49}Cr [Figs. 7(a) and 8] shows a remarkable adherence to cross-conjugate symmetry, especially at spins approaching the maximum allowed for the $f_{7/2}$ shell. In the even nuclei (Figs. 1 and 2), the symmetry is also reflected in the level energies, while for the odd pair (Figs. 3 and 4), this is less evident. In each nucleus, the $B(E2)$ values at moderate spins are somewhat larger than

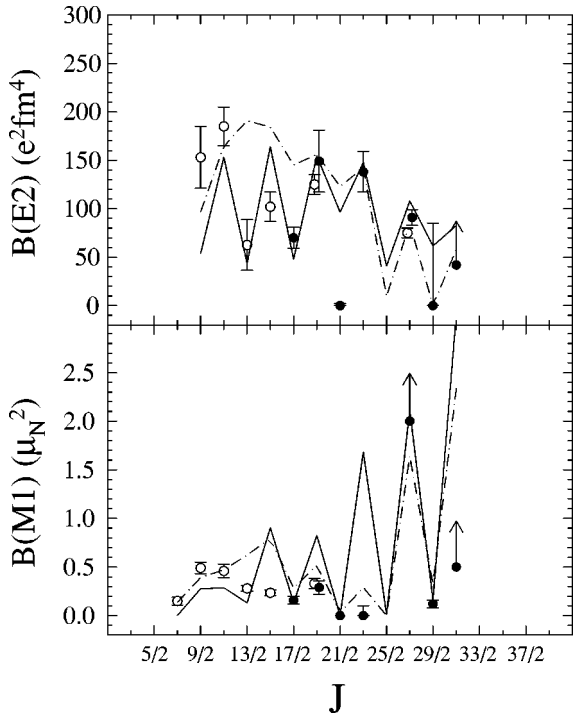

FIG. 9. Reduced rates for yrast transitions in ^{49}Cr. Open circles: Refs. [7,13]. Other details as in Figs. 5 and 6.

those predicted by an $f_{7/2}^k$ model (solid line [2]), but fall to these values near the maximum spin allowed in that configuration space, namely,

$$J_{\max}=\frac{1}{2}[n_p(8-n_p)+n_n(8-n_n)].$$

For single (neutron) particle-hole excitations to the $f_{5/2}p$ shell, $J_{\max}$ increases by n_n-2 (2 for ^{46}Ti and ^{47}V, 3 for ^{49}Cr, and 4 for ^{50}Cr). In the case of ^{48}Cr, discussed in Ref. [17], the admixture of $p_{3/2}f_{5/2}p_{1/2}$ configurations was necessary to obtain the rotorlike energies and sufficient $E2$ enhancement at low spin [23], but some features suggesting relative $f_{7/2}$ purity, such as low $B(E2)$ values, remain as the spin nears the maximum allowed by this shell alone. This is not surprising, since the lower angular momentum of the upper fp levels allows few contributions to the wave functions of the highest-spin states. In these nuclei neighboring ^{48}Cr, the $f_{7/2}$ model [2] appears to reproduce well both the magnitude and spin variations of the reduced transition rates at higher spin, while the fp excitations seem still to be required to account for the $E2$ rates at lower spin. In ^{50}Cr, where this has been most studied, shell model calculations involving a few particle-hole excitations to the upper fp shell [22], shown as dashed lines in Fig. 7, and full fp calculations [25], the dash-dotted lines, reproduce the general $E2$ enhancement as well as idiosyncracies such as the very small $12^+\rightarrow 10^+$ rate.

The oscillation in $B(M1)$ values near $J_{\max}$ can be understood with reference to the $f_{7/2}$ wave functions. In Ref. [2] these are given in the n-p formalism and are characterized by $\{J_p v_p, J_n v_n\}$, the total angular momenta, and seniorities of the proton and neutron subshells. For three like $f_{7/2}$ nucle-

ons, $J=\frac{15}{2},\frac{11}{2},\frac{9}{2},\frac{7}{2},\frac{5}{2},\frac{3}{2},\frac{1}{2}$, while for four $J=8,6,5,4,4^*,2,0$. Therefore, both $|J_{\max}\rangle$ and $|J_{\max}-1\rangle$ arise entirely from the same configuration $\{J_{p\max},J_{n\max}\}$ and the $M1$ transition is strong. The next states in descending spin, $|J_{\max}-2\rangle$ and $|J_{\max}-3\rangle$, consist mainly of $\{J_{p\max},J_{n\max}-2\}$ (and, in the odd-A case, $\{J_{p\max}-2,J_{n\max}\}$). These components are not connected to $\{J_{p\max},J_{n\max}\}$ by the $M1$ operator. So the $J_{\max}\rightarrow J_{\max}-1$ and $J_{\max}-2\rightarrow J_{\max}-3$ decays are strong while the intervening $J_{\max}-1\rightarrow J_{\max}-2$ transition is very weak, depending on minor components of the wave functions.

In the odd-A pair, there is a strong signature dependence at high spin for the $B(E2)$'s. Since the $\frac{31}{2}^-$ and $\frac{29}{2}^-$ states are both composed from the maximum alignments $\{\frac{15}{2},8\}$, the $E2$ selection rules alone cannot produce this effect, which must arise from matrix element cancellation.

What also seems evident is that below the band termination, the decay strength is concentrated in the yrast levels. Only in the case of ^{50}Cr is much structure seen above $J_{\max}$, where several routes of comparable intensity lead to the highest ''$f_{7/2}$ states.'' With the opening of the upper pf shell, many more states with spins 13 and higher are created. It appears, from the present study and from the more sensitive experiment at Legnaro [19], that these levels are not strongly mixed, since their paths of decay into the $f_{7/2}$ states differ markedly. It is also notable that the $E2$ transition strength, which falls as the even-spin states rise toward the $f_{7/2}$-band termination, reappears in the odd-spin states above this.

The present measurements lend some support for the view of the ''opposite-parity band'' in ^{47}V as a $d_{3/2}$ proton hole in ^{48}Cr. This may be seen in the backbend at the $\frac{27}{2}^+\rightarrow\frac{23}{2}^+$ transition, just $\frac{3}{2}\hbar$ above the backbend in ^{48}Cr at $12^+\rightarrow 10^+$ [14,18]. Further, the $B(E2)$ rates found in the positive-parity band of ^{47}V [Fig. 6(b)] are close to those found in ^{48}Cr for spins lower by $\frac{3}{2}$. On the other hand, the values of $B(M1)$ in this band are about an order of magnitude smaller than those in the respective ''$f_{7/2}$ bands.'' A similar relationship exists between the negative-parity bands of ^{46}Ti [Fig. 5(b)] and ^{47}V. These bands would not be expected to show an ''$f_{7/2}$ termination'' until $\frac{35}{2}^+$ and 17^-, respectively.

Lifetime measurements are important clues to the structure of states in the cases studied here. Earlier measurements with lighter projectiles [4,5,7,8] have provided good values for levels with spins up to 6 or 8. Other heavy-ion experiments have measured higher levels in ^{46}Ti [4] and in ^{49}Cr [13]. What remains to be explored are those levels a few $\hbar$ beyond the $f_{7/2}$-shell band termination, now accessible to shell model technology. In these and in the present measurements, states at intermediate spin are fed almost entirely from higher levels in the band, and have large uncertainties as a result. There is therefore in some cases (e.g., ^{47}V and ^{50}Cr) *terra incognita* in the lifetime measurements which is calling for further exploration.

ACKNOWLEDGMENTS

Thanks are due to M. A. Bentley for suggesting some of the alterations in the ^{49}Cr level structure, and for sharing his results prior to publication, to S. Lenzi and F. Brandolini for sharing the ^{50}Cr data from Legnaro, and to A. Poves for discussions of the fp-shell model calculations. L. Zamick has kindly shared unpublished calculations of ^{46}Ti, ^{50}Cr, and ^{49}Cr high-spin levels. The excellent technical help available at TASCC is much appreciated. The work was supported by grants from the Natural Science and Engineering Research Council of Canada.

[1] J. D. McCullen, B. F. Bayman, and L. Zamick, Phys. Rev. **134**, B515 (1964).
[2] W. Kutschera, B. A. Brown, and K. Ogawa, Riv. Nuovo Cimento **1**, 12 (1978).
[3] A. Yokoyama and H. Horie, Phys. Rev. C **31**, 1012 (1985).
[4] L. K. Peker, Nucl. Data Sheets **68**, 271 (1993).
[5] T. W. Burrows, Nucl. Data Sheets **74**, 1 (1995).
[6] T. W. Burrows, Nucl. Data Sheets **68**, 1 (1993).
[7] T. W. Burrows, Nucl. Data Sheets **76**, 191 (1986).
[8] T. W. Burrows, Nucl. Data Sheets **75**, 1 (1995).
[9] J. A. Cameron, D. G. Popescu, and J. C. Waddington, Phys. Rev. C **44**, 2358 (1991).
[10] J. A. Cameron, M. A. Bentley, A. M. Bruce, R. A. Cunningham, W. Gelletly, H. G. Price, J. Simpson, D. D. Warner, and A. N. James, Phys. Lett. B **235**, 239 (1990).
[11] J. A. Cameron, M. A. Bentley, A. M. Bruce, R. A. Cunningham, W. Gelletly, H. G. Price, J. Simpson, D. D. Warner, and A. N. James, Phys. Rev. C **44**, 1882 (1991).
[12] J. A. Cameron, M. A. Bentley, A. M. Bruce, R. A. Cunningham, H. G. Price, J. Simpson, D. D. Warner, A. N. James, W. Gelletly, and P. Van Isacker, Phys. Lett. B **319**, 58 (1993).
[13] A. A. Pakou, J. Billowes, A. W. Mountford, C. Terniero, and D. D. Warner, Phys. Rev. C **48**, 1573 (1993).
[14] J. A. Cameron, M. A. Bentley, A. M. Bruce, R. A. Cunningham, W. Gelletly, H. G. Price, J. Simpson, D. D. Warner, and A. N. James, Phys. Rev. C **49**, 1347 (1994).
[15] A. A. Pakou, J. Billowes, A. W. Mountford, and D. D. Warner, Phys. Rev. C **50**, 2608 (1994).
[16] J. L. Rodriguez, M.Sc. thesis, McMaster University, Hamilton, Canada, 1991 (unpublished).
[17] J. A. Cameron, J. Jonkman, C. E. Svensson, M. Gupta, G. Hackman, D. Hyde, S. M. Mullins, J. L. Rodriguez, A. Gallindo-Uribarri, H. R. Andrews, G. C. Ball, V. P. Janzen, D. C. Radford, D. Ward, T. E. Drake, M. Cromaz, J. DeGraaf, and G. Zwartz, Phys. Lett. B **387**, 266 (1996).
[18] S. M. Lenzi, D. R. Napoli, A. Gadea, M. A. Cardona, D. Hojman, M. A. Nagarajan, C. Rossi Alvarez, N. H. Medina, G. deAngelis, M. E. Debray, M. DePoli, S. Lunardi, and D. de Acuna, Z. Phys. A **354**, 117 (1996).
[19] S. M. Lenzi, C. A. Ur, D. R. Napoli, M. A. Nagarajan, D. Bazzacco, D. M. Brink, M. A. Cardona, G. de Angelis, M. De Poli, A. Gadea, D. Hojman, S. Lunardi, N. H. Medina, and C. Rossi Alvarez, Phys. Rev. C **56**, 1313 (1997).
[20] M. A. Bentley (private communication).
[21] P. Blasi, R. B. Huber, W. Kutschera, and C. Signorini, in *Proceedings of the International Conference on Nuclear Physics*,

Munich, 1973, edited by J. deBoer and H. J. Mang (North-Holland, Amsterdam, 1973), Vol. 1, p. 211.
[22] L. Zamick, M. Fayache, and D. C. Zheng, Phys. Rev. C **53**, 188 (1996); and (private communication).
[23] E. Caurier, A. P. Zuker, A. Poves, and G. Martinez-Pinedo, Phys. Rev. C **50**, 225 (1994).
[24] G. Martinez-Pinedo, A. Poves, L. M. Robledo, E. Caurier, F. Nowacki, J. Retamosa, and A. Zuker, Phys. Rev. C **54**, R2150 (1997).
[25] G. Martinez-Pinedo, A. P. Zuker, A. Poves, and E. Caurier, Phys. Rev. C **55**, 187 (1997).
[26] J. A. Cameron (unpublished).
[27] L. C. Northcliffe and R. F. Schilling, Nucl. Data Tables **7**, 233 (1970).
[28] A. E. Blaugrund, Nucl. Phys. **A88**, 501 (1966).
[29] J. F. Ziegler, J. P. Biersack, and U. Littmark, *The Stopping and Range of Ions in Solids* (Pergamon Press, New York, 1985).
[30] P. M. Endt, At. Data Nucl. Data Tables **23**, 547 (1979).
[31] N. R. F. Rammo, P. J. Nolan, L. L. Green, A. N. James, J. F. Sharpey-Schafer, and H. M. Sheppard, J. Phys. G **8**, 101 (1982); Nucl. Instrum. Methods **161**, 291 (1979).